

NASA TECHNICAL NOTE



NASA TN D-2893

NASA TN D-2893



MATERIAL DAMPING OF ALUMINUM BY A RESONANT-DWELL TECHNIQUE

by Neal Granick and Jesse E. Stern

Goddard Space Flight Center

Greenbelt, Md.

NATIONAL AERONAUTICS AND SPACE ADMINISTRATION • WASHINGTON, D. C. • AUGUST 1965

NASA TN D-2893

TECH LIBRARY KAFB, NM



0079611

MATERIAL DAMPING OF ALUMINUM BY A
RESONANT-DWELL TECHNIQUE

By Neal Granick and Jesse E. Stern

Goddard Space Flight Center
Greenbelt, Md.

NATIONAL AERONAUTICS AND SPACE ADMINISTRATION

For sale by the Clearinghouse for Federal Scientific and Technical Information
Springfield, Virginia 22151 - Price \$2.00

MATERIAL DAMPING OF ALUMINUM BY A RESONANT-DWELL TECHNIQUE

by

Neal Granick and Jesse E. Stern

Goddard Space Flight Center

SUMMARY

At intermediate and high stress levels, material damping has been considered stress-amplitude-dependent and contributions from frequency-dependent anelastic mechanisms have been considered negligible. These considerations are contradicted by the findings of this investigation for Aluminum 2024-T4. The relations between material damping, stress amplitude, and frequency were experimentally examined for this material by means of a resonant-dwell technique employing "identical" double cantilever reeds. Tests were run in air (760 mm, 70°F), and in vacuum (0.2 mm, 70°F), at stress amplitudes up to 20,000 psi and at frequencies from 15 to 1500 cps. Results showed that: damping as measured in air was largely aerodynamic drag and was displacement-amplitude and frequency dependent; damping as measured in vacuum was wholly material damping, independent of stress amplitudes up to 20,000 psi, and dependent on frequency; and there was agreement with the Zener theory of thermal relaxation.

CONTENTS

Summary	iii
INTRODUCTION	1
TEST SPECIMEN	4
TEST METHOD	5
Facilities and Instrumentation	5
Errors Due to External Damping	5
Measurement Errors	7
Damping and Resonant Frequency Differences	7
Determination of Resonant Frequency	8
Determination of Test Stress Levels	10
TEST PROCEDURE	11
Application of Optical Tracking Targets to Test Specimen . . .	11
Dynamic Beam Balance (Reed Tuning)	11
Test Run In Air	14
Test Run In Vacuum	14
RESULTS AND CONCLUSIONS	14
References	20
Appendix A—List of Symbols	21

MATERIAL DAMPING OF ALUMINUM BY A RESONANT-DWELL TECHNIQUE

by

Neal Granick and Jesse E. Stern

Goddard Space Flight Center

INTRODUCTION

Damping is an energy dissipative process which is manifested during the mechanical vibration of structural elements and systems. It is of particular interest to the dynamicist and designer who is concerned with the analysis and development of equipment which must function successfully and survive in a mechanically dynamic environment.

The damping of structural systems may be separated into three general types: joint damping arising from friction sliding and slapping of joint interfaces; air or fluid damping arising from loss or transmission of energy to the surrounding fluids; and material damping, an internal energy loss, arising from complex internal behavior of the material itself.

In order to design and predict the behavior of structural systems with greater accuracy, it is necessary to have quantitative damping information. This paper is a report on the quantitative evaluation of material damping of aluminum. Aluminum was selected for initial investigation since it is extensively used as a structural material for spacecraft. Other materials will be investigated in the near future.

Considerable effort has been made in experimentally determining the material damping properties of metals subject to vibration. Most metals investigated have exhibited a non-linear dependence of material damping with respect to vibration amplitudes and, in some cases, have also exhibited a dependence on frequency. Crandall (Reference 1) investigated the problem of material damping and proposed the following relations,

$$g = \left(\frac{S}{S_0} \right)^n \quad (1)$$

and

$$g = \left(\frac{S}{S_0} \right)^n \frac{\omega\tau}{1 + \omega^2\tau^2} \quad (2)$$

where

- g = material damping coefficient,
- S = stress amplitude,
- ω = vibration frequency (radians),
- τ = relaxation time for temperature equalization in a specimen by transverse heat flow,
- $S_{0,n}$ = material constants.

The frequency dependent term in Equation 2 was suggested by Zener's relation (Reference 2)

$$g = \frac{\alpha^2 ET}{c} \left(\frac{\omega \tau}{1 + \omega^2 \tau^2} \right) \quad (3)$$

when

$$\tau = \frac{h^2 c}{\pi^2 k} \quad (3a)$$

for a flat beam of uniform thickness, where

- α = coefficient of linear expansion,
- c = specific heat per unit volume,
- E = modulus of elasticity,
- T = absolute temperature,
- h = thickness of cantilever beam,
- k = thermal conductivity.

From Equations 1 and 2, Crandall derived explicit relations for evaluating the specimen damping coefficient of a cantilever beam at its first mode resonance,

$$g_s = R^{\frac{1}{n+1}} \left(\frac{2.71 \sqrt{\rho E}}{S_0} \frac{a}{\omega_1} \right)^{\frac{n}{n+1}}, \quad (4)$$

and

$$g_s = R^{\frac{1}{n+1}} \left(\frac{2.71 \sqrt{\rho E}}{S_0} \frac{a}{\omega_1} \right)^{\frac{n}{n+1}} \left(\frac{\omega_1 \tau}{1 + \omega_1^2 \tau^2} \right)^{\frac{1}{n+1}}, \quad (5)$$

where

- ρ = mass density of beam material,
- a = acceleration amplitude of beam root,
- ω_1 = first mode resonant frequency,
- R = f (material, mode shape),
- g_s = specimen damping coefficient related to g by

$$g_s = gR . \quad (6a)$$

Crandall also showed that

$$g_s = \frac{1}{Q} , \quad (6b)$$

and for a cantilever beam

$$Q = \frac{\delta_r}{1.566 \delta_0} , \quad (6c)$$

where

Q = magnification factor at resonance,

δ_0 = input root displacement at resonance,

δ_r = output tip displacement at resonance.

For a given material, geometry and mode shape R , ρ , E , S_0 , n , and τ are constants and Equations 4 and 5 reduce to

$$g_s = K \left(\frac{a}{\omega_1} \right)^{\frac{n}{n+1}} , \quad (7)$$

and

$$g_s = K \left(\frac{a}{\omega_1} \right)^{\frac{n}{n+1}} \left(\frac{\omega_1 \tau}{1 + \omega_1^2 \tau^2} \right)^{\frac{1}{n+1}} . \quad (8)$$

If the relaxation time τ is large such that $\omega_1^2 \tau^2 \gg 1$, then Equation 8 reduces to

$$g_s = K' \frac{a^{\frac{n}{n+1}}}{\omega_1} , \quad (8a)$$

where

$$K' = K \left(\frac{1}{\tau} \right)^{\frac{1}{n+1}} . \quad (8b)$$

Equations 6, 7, and 8 show that: the specimen damping coefficient can be determined by measuring the magnification factor at resonance; the material constant, n , can be evaluated by measuring the slope of a log-log plot of g_s vs. a/ω_1 for Equation 7, and $g_s \omega_1$ vs. a for Equation 8a; and S_0 can be computed when n has been determined.

A check of Equations 7 and 8a against data taken by Vet (Reference 3) correlated well with Equation 7 for steel and brass but failed for aluminum, and correlated well with Equation 8a for aluminum but failed for steel and brass. Vet's data included air damping and probably some joint damping. To evaluate more accurately the validity of Crandall's proposed relationships, damping tests were run which eliminated, minimized, or accounted for these external effects. This was accomplished by testing in air and in a vacuum, and by developing improved test techniques.

TEST SPECIMEN

The test method selected for this investigation was a steady state excitation of a cantilever beam by an electromagnetic vibrator.

Before selecting a beam configuration, consideration was given to two problems affecting the dynamic behavior of the vibrating system: joint damping at the beam-vibrator table interface, and the generation of an undesired rocking mode on the beam-vibrator table system.

An examination of the single reed cantilever in Figures 1b, 1c and 1d shows that a moment reaction, M'_B , at the fastener, will always exist and have a value equal to or greater than the root moment, M' . The moment, M'_B , increases the probability of joint damping. Further, to prevent a rocking mode it is necessary that $F'd' = M'$. To satisfy this relation, the beam must be positioned by a time consuming, trial and error process until rocking is eliminated.

An examination of the double reed cantilever in Figures 1b, 1c and 1d shows that if $F_1 = F_2$, $M_1 = M_2$, and F_1 and F_2 are equidistant from and parallel to the elastic axis, then, M_B , the moment reaction at the fastener, vanishes and the probability of joint damping is reduced. Further, the sum of the moments $(F_1d_1 - F_2d_2 - M_1 - M_2)$ also vanishes and the causes of rocking are eliminated. This is achieved by a double reed cantilever beam in which the geometry of both reeds is identical and the center of the base block is located on the geometric center of the vibrator table. For a well designed table the geometric center is coincident with the elastic axis, the center of gravity of the vibrator table, and the resultant electromagnetic driving force. For these reasons, the double reed cantilever beam was chosen for the test beam configuration.

Adequacy of the test specimen depends upon an ability to carefully fabricate each reed to the same geometry in order to have an identical and symmetrical response. In practice, there will always exist a small difference in "identical" reeds due to manufacturing techniques. To overcome this problem, the reeds were manually tuned to the same frequency. This was accomplished by exciting the beam specimen, observing the resonant frequencies of both reeds, and then placing additional mass on the tip of the reed exhibiting higher resonance until the resonant frequencies of both reeds were equal.

The test specimens were designed with first bending mode resonances in the frequency range 15-1500 cps. Length to width ratios of at least 6:1 helped minimize the effects of Poisson's ratio. Reed thickness for some specimens was varied to determine the effect of the relaxation time, τ .

Finally, the root radius was chosen equal to the reed thickness. This choice was based on a compromise which provided a stress concentration factor of only 1.1 with a minor effect on the length and crosssectional properties of the beam.

A number of restrictions were placed on the methods used to control material homogeneity and finished. For uniformity, all of the specimens were cut from a single bar stock of 2024-T4 aluminum material. Machining tolerances were held to $\pm .001$ inch on reed thickness and to $\pm .005$ inch on reed length and root radius.

Machining of the beams was done in successively reduced depths of cut so that final material surfaces would be as free as possible of residual machining stress. For example, the last four cuts were only .001, .001, .0005 and .0005 inch thick, respectively. The final operation was to hand polish the reeds to an 8 RMS surface finish. Specimens were inspected for conformity to these tolerances prior to test.

Table 1 lists beam geometries, dimensions, and resonant frequencies of test specimens.

TEST METHOD

Facilities and Instrumentation

Table 2 lists the major items used in the experimental test set-up.

Errors Due to External Damping

Material damping is an internal energy loss process. In order to accurately measure its value it is necessary to eliminate, reduce, or account for damping contributed from external sources.

External damping arises from three sources: joint damping, eddy current damping, and air damping. Joint damping is virtually eliminated by securely clamping the beam specimen to the

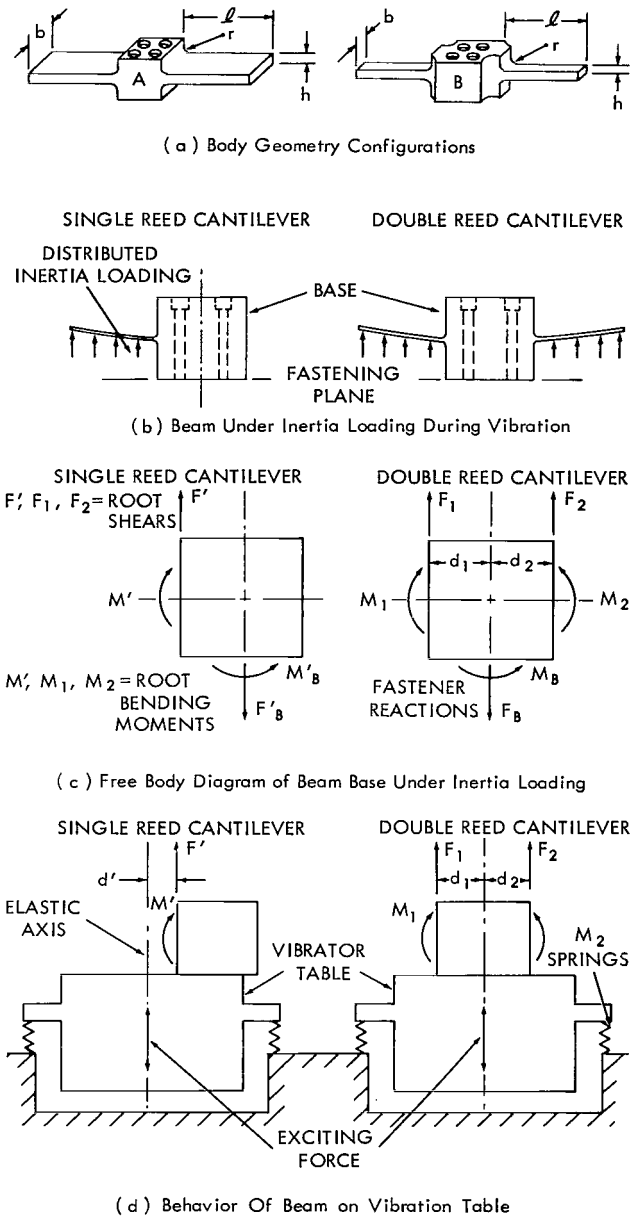


Figure 1—Comparison of the behavior of single and double reed cantilever beams subject to vibration.

Table 1
Beam Geometry

Beam Configuration*	Thickness h in.	Width b in.	Length l in.	Radius r in.	First Mode Frequency cps (Nominal)
A	.100	1.000	14.758	.100	15
A	.100	1.000	10.436	.100	30
A	.100	1.000	6.832	.100	70
B	.100	.500	4.667	.100	150
B	.100	.500	3.300	.100	300
B	.100	.250	2.161	.100	700
B	.100	.250	1.476	.100	1500
B	.050	.250	2.334	.050	300
A	.200	1.000	9.334	.200	75

*Refer to Figure 1(a) for beam geometry.

Table 2
Instrumentation Test Equipment

Item	Mfr	Model	Characteristics
Accelerometer	Endevco	2217	
Amplifier, Double Integrator ("Dial-a-Gain")	Unholtz-Dickie	610R	
Amplifier, Input	Endevco	2614B	
Displacement Follower, Optical	Optron	701	Freq. Response = Flat from DC to 3 kc Displacement Range = 12 μ in. to 2 in.
Exciter, Vibration	Unholtz-Dickie	100	Vector Force = 225 lbs. max. Frequency Range = 5-5000 cps
Oscillator, Stable Amplitude, Ultra-Low Distortion	Krohn-Hite	446	Frequency Range = 1 cps - 100 kc Amplitude Stability = $\pm 0.01\%$ Harmonic Distortion = $\pm 0.02\%$ Live Frequency Modulation = $\pm 0.01\%$
Oscilloscope, Dual-Beam	Tektronix	502	
Power Supply	Endevco	2623	
Power Supply, Displacement Follower	Optron	702	
Power Supply, Vibration Exciter, DC Storage Battery	Rebat	R-35	Output Volts = 12 Ampere - Hours = 35
Voltmeter, AC, True RMS	Ballantine	320	Voltage Range = 100 μ v to 320 volts Frequency Range = 5 cps to 4 Mc

vibrator table and by eliminating, through design, conditions which foster excessive loads on the joint. Eddy current damping arises from the movement of the beam in the magnetic field of the electrodynamic exciter. Tests were run in which the dc field current of the exciter was varied from 10 to 40 amperes. No measurable change in response was observed under these conditions. Therefore, the eddy current damping was negligible in these tests. All subsequent tests were run with an 8 ampere field current. Air damping and energy transfer to the air was eliminated by testing in a vacuum.

Measurement Errors

Previously, it was shown that the specimen damping coefficient was related to the magnification factor at resonance. Therefore, any errors in producing and measuring the input and output amplitudes must be eliminated. This requires a translational rigid body response of the beam-vibrator table system in the direction of the exciting force. The appearance of a coupled rocking mode on the system presents two problems: evaluating the relation between the input excitation and the output amplitudes of the reeds, and measuring the amount of beam energy transferred to or dissipated in the vibrator table support system. The use of the tuned double-reed cantilever beam described earlier virtually eliminated these problems.

Since material damping is small a high Q may be expected. From Equation 6c it can be seen that errors in measuring δ_o and δ_r are critical, particularly with respect to δ_o which may be orders of magnitude smaller than δ_r . The input displacement, δ_o , was derived by measuring the input frequency and acceleration with a calibrated, high sensitivity, high signal-to-noise ratio, accelerometer-amplifier system. The system sensitivity was 500 mv/g; the system noise level was about 2 millivolts; and the lowest measured signal during the tests was approximately 20 millivolts for an acceleration of about 0.04g. The accuracy of this measurement technique was about $\pm 3\%$ of reading. Ripple in the input displacement was eliminated by energizing the vibrator field with direct current from storage batteries rather than by a rectified alternating current supply.

Reed tip displacements were measured by a massless non-contact method of measuring tip displacement, using optical displacement followers. The displacement followers provided an electrical signal proportional to displacement, permitting simultaneous measurement and comparison of the two reed tip motions on a meter-oscilloscope arrangement. It was also possible to compare input and output motions. The accuracy of the displacement follower measurement system was about 1% of full scale. Measurements taken during this investigation were repeatable within 4.5%.

Damping and Resonant Frequency Differences

An analog computer study* was made to determine the effects on reed motion caused by differences in damping and resonant frequencies between the two reeds. The results showed that: a

*Heine, J., "Analysis of a Model for the Experimental Determination of Damping," Private Communication.

1% damping difference produced about a 1-1/2% amplitude difference and no significant phase difference between the two reeds; a 0.1% resonant frequency difference produced about a 50% amplitude difference and about 60° phase angle difference between reeds; and for each reed the phase angle between input and output displacements rapidly changed at frequencies very close to the resonant frequency of each reed.

This study indicated that it is critical for each reed to have the same natural frequency if valid data are to be obtained. It also indicated that the phase angle difference between the two reeds can be used as a highly accurate means of tuning the reeds to the same frequency.

Determination of Resonant Frequency

The natural frequencies of the reeds must be experimentally determined before material damping data is obtained. During this determination it was observed that two significant frequencies appeared: a "notch" frequency at which the input (root) amplitude reached a minimum for a fixed input force amplitude, and a "peak" frequency at which the output (tip) amplitude reached a maximum for the same fixed force input amplitude (see Figure 2). The difference between these frequencies was small. It was also observed that large differences in the magnification factor existed when the reeds were excited at the "notch" or "peak". This raised the questions, "What are the 'notch' and 'peak' frequencies," and "At what frequency do we excite the test specimen?"

To answer these questions a simplified analysis was performed. The following assumptions were made: the beam-vibrator table system is a two degree of freedom system with lumped parameters, the system is responsive only in translational modes, and damping is neglected since it is very small and has no effect on resonant frequencies. A schematic arrangement of the system is shown in Figure 3. The differential equations of motion for the system are:

$$M_v \ddot{x}_v + (k_v + k_b) x_v - k_b x_b = P_0 \sin \omega t , \quad (9a)$$

$$M_b \ddot{x}_b + k_b (x_b - x_v) = 0 . \quad (9b)$$

The solution to these equations is

$$x_v = \left\{ \frac{1 - \left(\frac{\omega}{\omega_b}\right)^2}{\left[1 - \left(\frac{\omega}{\omega_b}\right)^2\right] \left[1 + \frac{k_b}{k_v} - \frac{\omega^2}{\Omega^2}\right] - \frac{k_b}{k_v}} \right\} \frac{P_0}{k_v} \sin \omega t \quad (10a)$$

and

$$x_b = \left\{ \frac{1}{\left[1 - \left(\frac{\omega}{\omega_b}\right)^2\right] \left[1 + \frac{k_b}{k_v} - \frac{\omega^2}{\Omega^2}\right] - \frac{k_b}{k_v}} \right\} \frac{P_0}{k_v} \sin \omega t , \quad (10b)$$

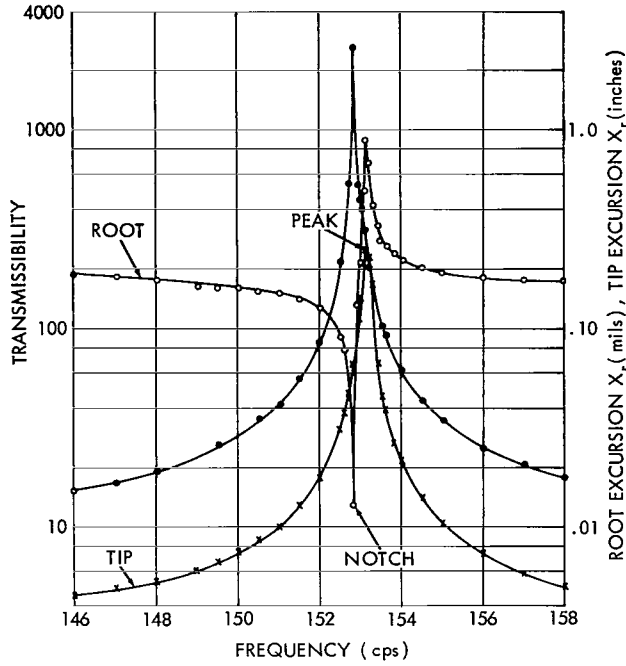


Figure 2—Transmissibility plot for a nominal 150 cps beam, 0.10 in. thick (specimen No. A-10).

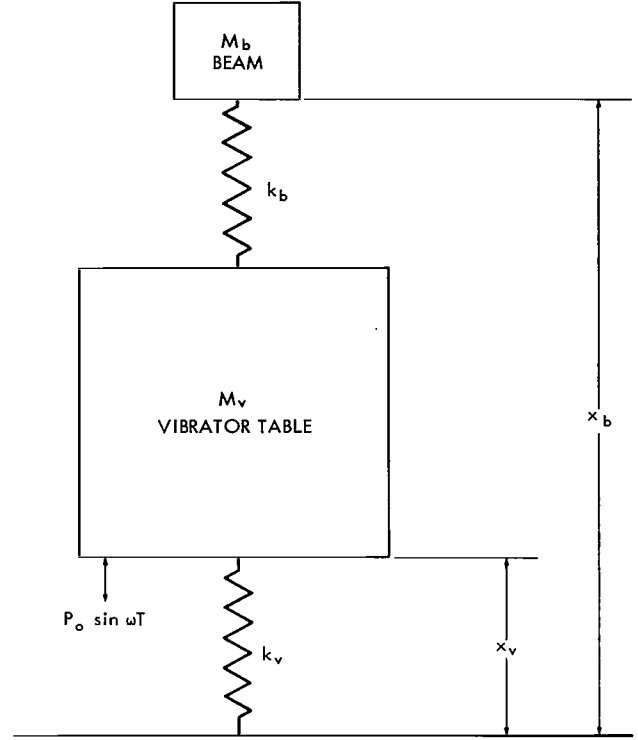


Figure 3—Model for the analysis of a beam-vibrator combination as a two-degree-of-freedom system.

where

ω = exciting frequency,

$\omega_b = \sqrt{\frac{k_b}{M_b}}$ = natural frequency of the beam,

$\Omega = \sqrt{\frac{k_v}{M_v}}$ = natural frequency of the vibrator table assembly,

x_v = displacement of M_v with respect to ground,

x_b = displacement of M_b with respect to ground.

By setting the denominators of Equations (10a) and (10b) equal to zero the following expression is obtained:

$$\omega^2 = \frac{\omega_b^2}{2} \left\{ \left[1 + \frac{\Omega^2}{\omega_b^2} \left(1 + \frac{k_b}{k_v} \right) \right] \pm \sqrt{\left[1 + \frac{\Omega^2}{\omega_b^2} \left(1 + \frac{k_b}{k_v} \right) \right]^2 - 4 \frac{\Omega^2}{\omega_b^2}} \right\}. \quad (11)$$

Equation (11) identifies two system resonant frequencies, each different from Ω or ω_b . One of these system resonant frequencies is close to the natural frequency ω_b . This is the "peak" frequency.

It has been shown that Q is related to the specimen damping coefficient by

$$g_s = \frac{1}{Q} .$$

Q is defined as the magnification factor at resonance or the maximum magnification factor. The magnification factor, F , for the beam is

$$F = \frac{x_b - x_v}{x_v} = \frac{\left(\frac{\omega}{\omega_b}\right)^2}{1 - \left(\frac{\omega}{\omega_b}\right)^2} \quad (12)$$

and

$$Q = F_{max} = \infty \text{ at } \omega = \omega_b .$$

It can also be seen from Equation 10a that $x_v = 0$ when $\omega = \omega_b$. Hence, ω_b can be identified as the "notch" frequency; and data on damping characteristics must be obtained at this frequency, where the table's vibration amplitude is at a minimum.

Determination of Test Stress Levels

Defining the relation between damping and stress amplitudes was one of the major objectives of this investigation. The use of strain gages suggested a simple and effective method for measuring the stresses, but was discarded because it might have introduced additional and uncertain damping from the adhesive joint and from the gage backing material. It was decided that root stresses could best be evaluated by measuring the dynamic displacement of a particular point on the cantilever reed, generally the tip, and computing the stresses from the equations of dynamic displacement (Reference 4):

$$\delta_x = \frac{w\ell^4}{8EI} \left[\frac{1}{2} \left(\cosh 1.875 \frac{x}{\ell} - \cos 1.875 \frac{x}{\ell} \right) - .368 \left(\sinh 1.875 \frac{x}{\ell} - \sin 1.875 \frac{x}{\ell} \right) \right] \quad (13)$$

$$M_r = EI \left(\frac{d^2 \delta_x}{dx^2} \right)_{x=0} = \frac{(1.875)^2}{8} w \ell^2 \quad (14)$$

$$\sigma_r = \frac{M_r \frac{h}{2}}{I} = \frac{1.76 h E \delta_x}{\ell^2 \left[\frac{1}{2} \left(\cosh 1.875 \frac{x}{\ell} - \cos 1.875 \frac{x}{\ell} \right) - .368 \left(\sinh 1.875 \frac{x}{\ell} - \sin 1.875 \frac{x}{\ell} \right) \right]} \quad (15)$$

where

δ_x = displacement of cantilever at a distance x from the root.

M_r = bending moment at root,

σ_r = stress at cantilever root,

l = reed length,

h = reed thickness.

w = weight of beam per unit length.

In order to experimentally check the stress, σ_r , as computed by Equation 15, several of the reeds were instrumented with strain gages after the damping tests were run. These were located on the flat portion of the beam near the root radius. The reeds were excited at predetermined amplitudes, δ_x , and the measured stresses were observed. The stresses computed from Equation 15 were within 5% of the measured stresses. This indicated that the technique of indirect stress measurement was satisfactory and reasonably accurate.

TEST PROCEDURE

Figure 4 shows the instrumentation block diagram; Figure 5 a typical test setup; and Figure 6 beams for each resonant frequency.

Application of Optical Tracking Targets to Test Specimen

Beam specimens were cleaned with acetone or trichlorethylene to remove all dirt and oil film. Adhesive backed targets were cut to a height equal to the thickness of the reeds and to a width of 1/8 inch. Four targets were applied to the tips of the reeds as shown in Figure 7. Where the tip amplitudes of the reeds were expected to exceed the range of the optical displacement follower, the targets were moved a known distance in from the tip. The displacement of this point is related to the tip displacement through the bending curve equation. Four symmetrically located targets were used to limit unbalance in the reeds.

Dynamic Beam Balance (Reed Tuning)

After the targets were attached, the test specimen was fastened to the vibrator table by

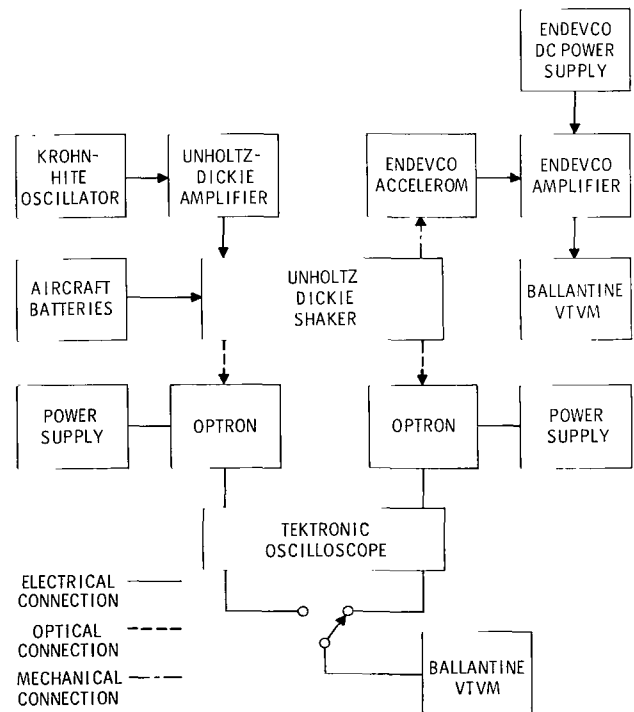


Figure 4—Instrumentation block diagram.

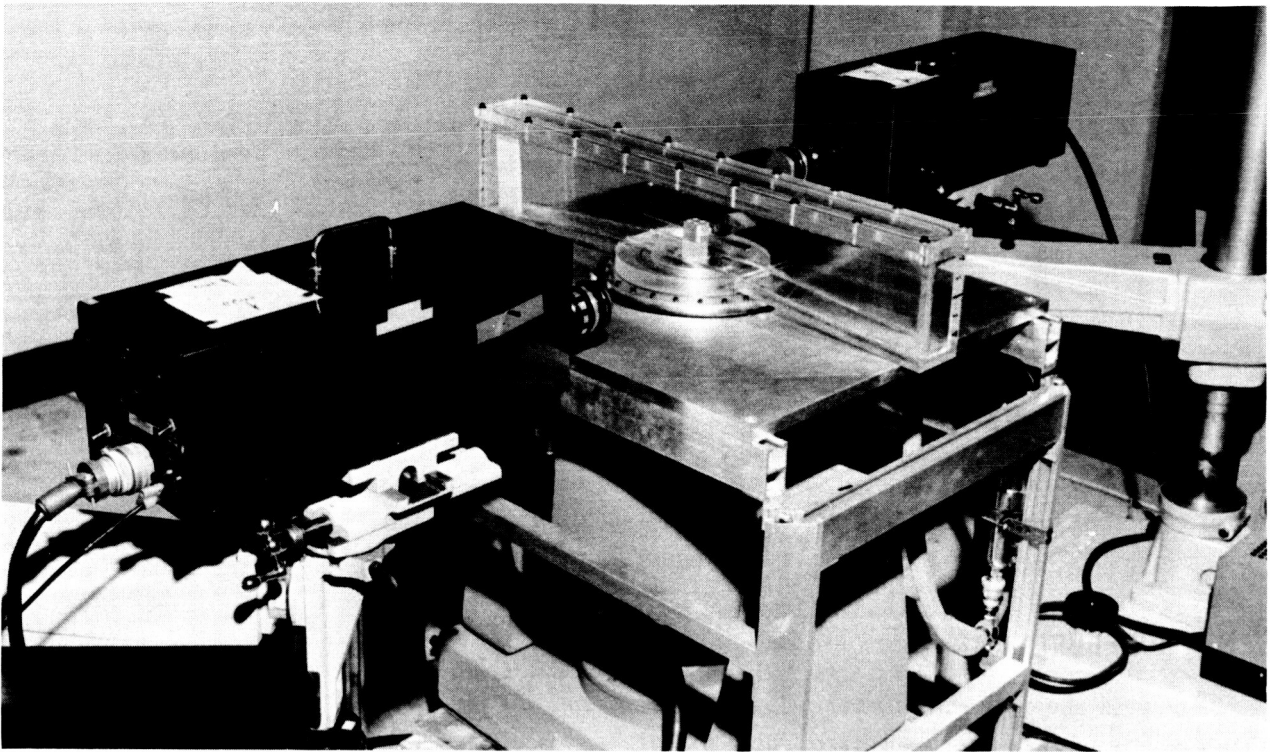


Figure 5—Typical measurement test setup.

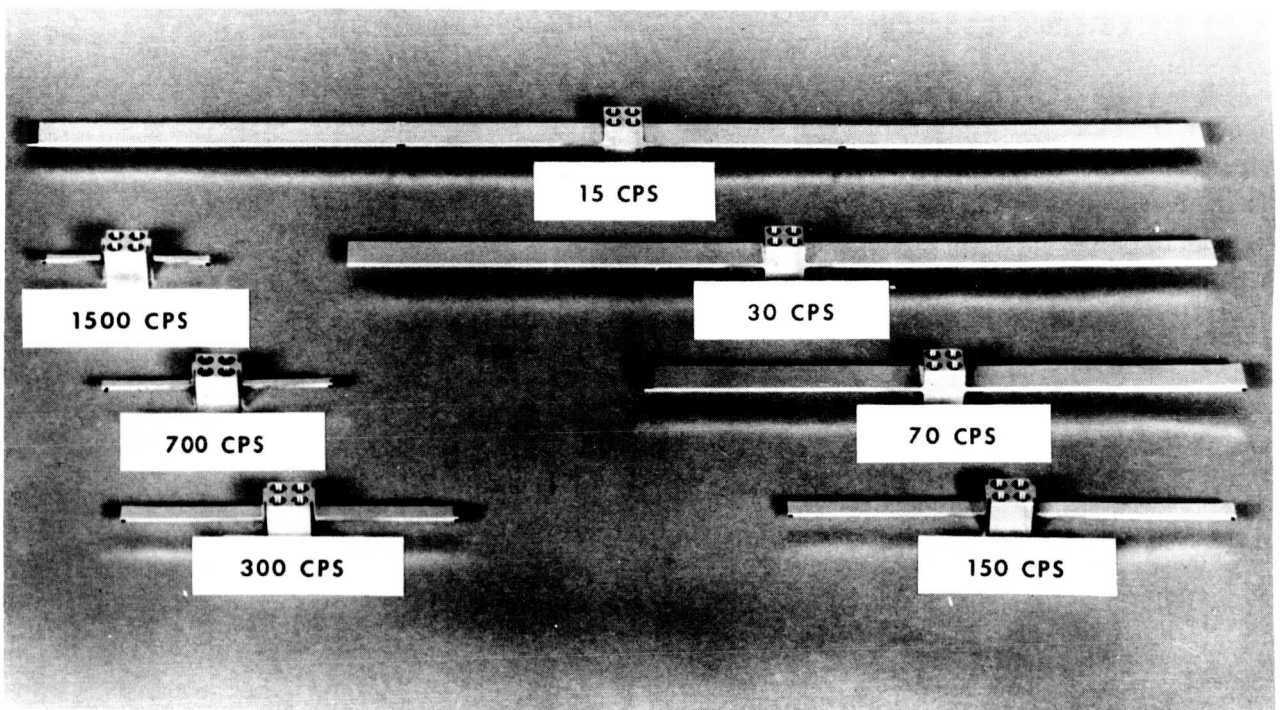


Figure 6—Beams for each measurement frequency.

four #10 cap screws with about 20 inch pounds torque per screw. Two were optical displacement followers focussed or "locked on" the targets, one at each reed. The output of the displacement followers was fed into a dual beam oscilloscope. The following was then performed:

1. The test specimen was excited with a low level, fixed-force amplitude through a frequency range of about 5% below and above the calculated natural frequency of the reeds.

2. The displacement follower output signals were observed on the oscilloscope noting the frequency at which each reed reached its maximum amplitude and the phase angle between amplitudes as each reed passed through its maximum amplitude (Figure 8). If the phase angle was zero the two reeds were tuned to the same natural frequency.

3. Where a phase angle existed a trial mass was added to the tip of the higher natural frequency reed and steps (1) and (2) were repeated.

4. If a phase angle still existed after step (3), additional mass was added or previously added mass was removed until the phase angle was zero, indicating that the reeds were tuned to the same natural frequency. The addition or removal of mass was determined by the magnitude and shift in the phase angle (Figure 8 (b and c)).

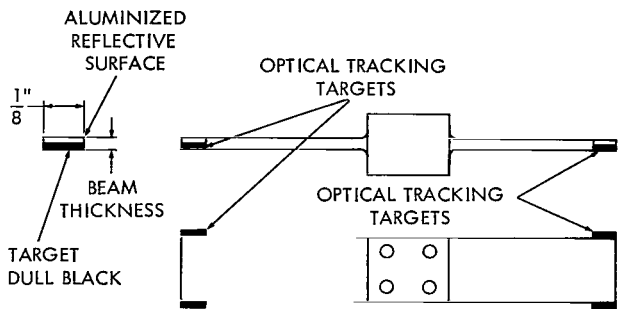


Figure 7—Location of optical tracking targets.

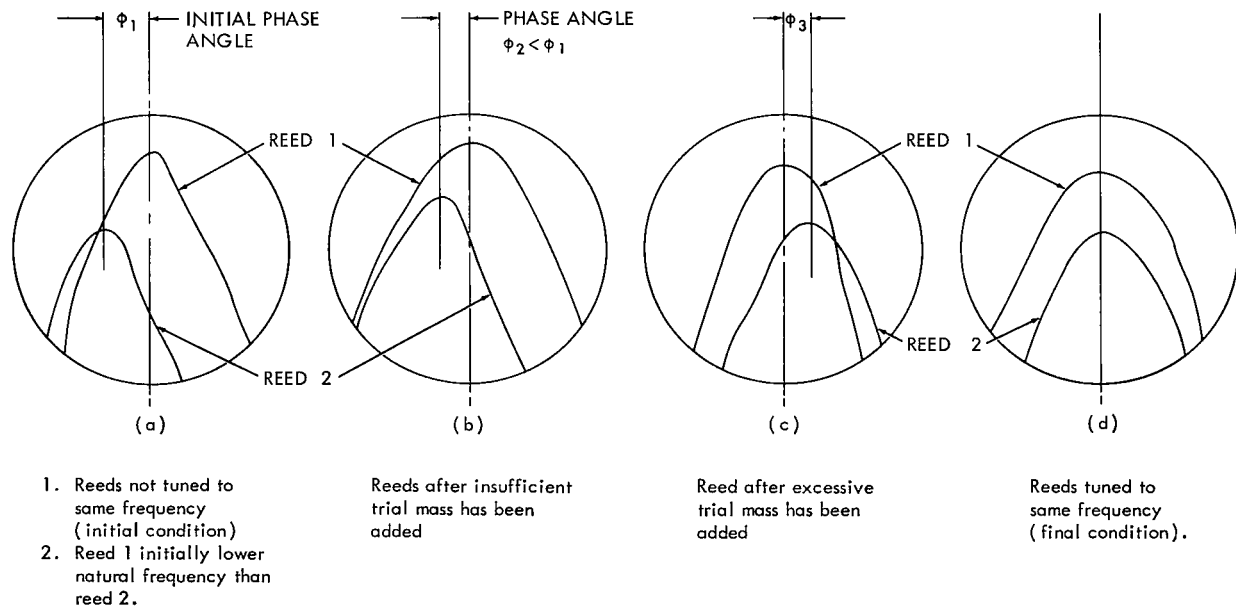


Figure 8—Reed tip displacement as seen on dual-beam oscilloscope.

The added masses consisted of small pieces of plastic electrical tape about 1/16 inch square, symmetrically located on the reed tip to prevent twist under dynamic conditions. The masses were placed at the tip where they were most effective dynamically and where they least affected the specimen damping.

When the reeds were tuned to the same frequency the displacements were in phase and the peak amplitudes were within 3% of each other.

Test Run in Air

(a) Predetermined root stress levels were selected at which the tests were to be performed. The stresses covered the range of 5000-20,000 psi in increments of 5000 psi. Reed amplitudes at the target locations were computed from these root stresses.

(b) The accelerometer was attached to the vibration table adjacent to the base block of the tuned test specimen. The displacement followers were "locked on" the reed targets and instrumentation was hooked up as shown in Figure 4. The "notch" frequency was located by exciting the test specimen with a very low constant-force amplitude.

(c) The double integrator amplifier was adjusted until the predetermined amplitude at the target was obtained.

(d) Root acceleration, target displacement, and excitation (notch) frequency were recorded as indicated on the rms voltmeter and oscillator.

(e) Steps (c) and (d) were repeated for each predetermined target amplitude.

Test Run in Vacuum

A specially designed vacuum chamber was installed over the test specimen and evacuated to 0.2 torr. Steps (c) through (e) above were repeated.

RESULTS AND CONCLUSIONS

A preliminary study was made to determine whether a stress limit existed beyond which the material damping properties suddenly or significantly changed behavior. A nominal 70 cps resonant cantilever beam was tested in a vacuum through the range of 15000 - 42000 psi root stress. The results are shown in Figure 9, Run 1. Immediately after Run 1, the beam was tested through the range of 8000 - 27000 psi root stress. These results are shown in Figure 9, Run 2.

From Run 1, it was observed that damping very slowly increased with stress amplitude between 20000 - 35000 psi but drastically changed above 35000 psi. From Run 2, it was observed that damping remained constant between 8000 - 20000 psi and noticeably increased with stress amplitude between 20000 - 27000 psi. Also, the damping in Run 2 had permanently increased in the lower stress amplitude range after the beam was subjected to the near yield stresses of Run 1.

Therefore, tests were limited to stress levels up to 20,000 psi to maintain the original material damping characteristics of the beams.

The results of the investigation for aluminum 2024-T4 are shown in Figures 10-15 and in Table 3 and Table 4. Figures 10-12 are plotted in accordance with the log form of Equation 8a,

$$\log g_s = \log \frac{K'}{\omega_1} + \left(\frac{n}{n+1} \right) \log a \quad (16)$$

Figure 13 is plotted in accordance with a modified log form of Equation 8a,

$$\log g_s \omega_1 = \log K' + \left(\frac{n}{n+1} \right) \log a \quad (17)$$

Figure 10 compares damping for a nominal 70 cps resonant frequency beam as measured in air at ambient pressures and in a vacuum of 0.2 torr, over the same stress amplitude range of 5000 to 20,000 psi. The "in air" plot shows the non-linear behavior of damping in air where the quantity n , has a value of 0.78 as calculated from the slope of the plot. This compares with 0.77 as reported by Crandall (Reference 1). The slope of the "in vacuum" plot is zero, hence the quantity n is zero, indicating that the damping in vacuum is independent of stress amplitude. It should be noted here that $g_s = g$ where $n = 0$ (see Reference 1).

Figure 11 shows the non-linear behavior of damping in air for the series of beams tested. It shows that damping is frequency and amplitude dependent. The amplitude dependence appears to be due to displacement or velocity and not to stress (Figure 12). The non-linear behavior then may be attributed to air damping.

Figure 12 shows the behavior of damping in vacuum for the same series of beams. The slopes of all the curves are zero, hence n is zero and stress amplitude independence is shown. The damping here is *material damping* only and its dependence on frequency is clearly evident.

Figure 13 further shows the independence of damping on stress amplitude and the constancy of the product $g_s \omega$.

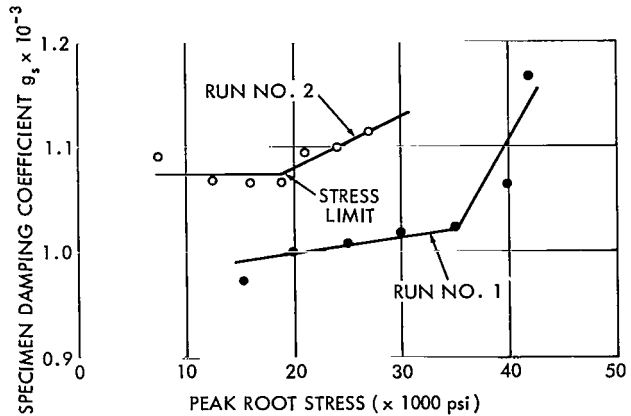


Figure 9—Graph showing the location of stress limit and the effect of near yield stresses on the damping coefficient.

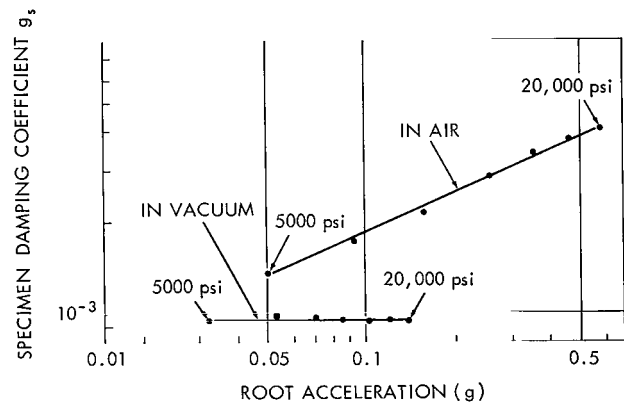


Figure 10—Comparison of damping in vacuum with damping in air for a nominal 70 cps beam stressed between 5000 and 20,000 psi at beam root.

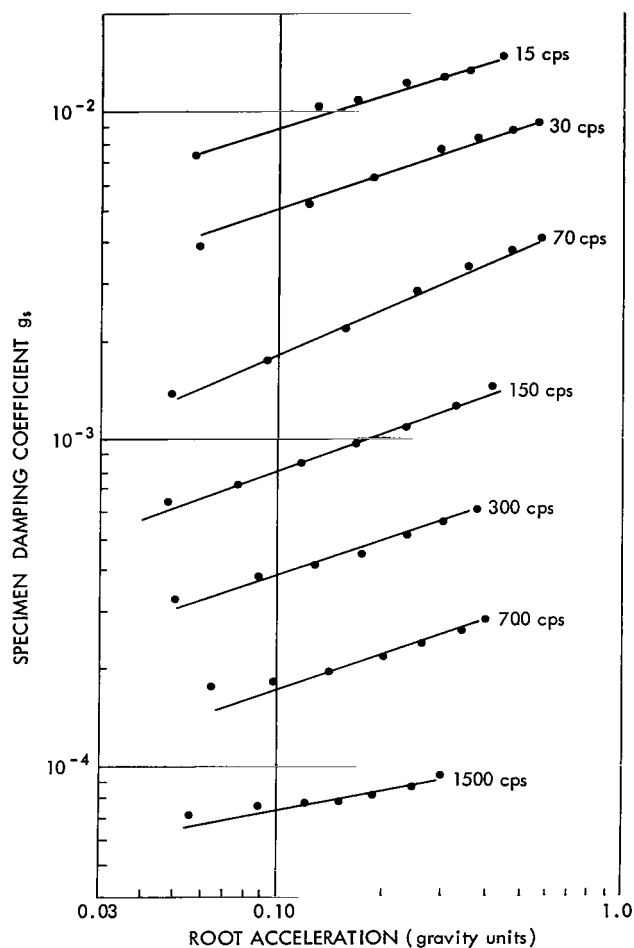


Figure 11—Results for damping in air for seven 1/10-inch thick aluminum cantilever beams (resonant frequencies shown).

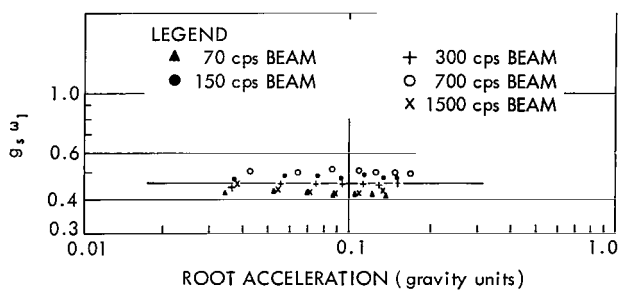


Figure 13—Results for five resonant beams of 1/10-inch thick aluminum tested in a vacuum of 0.2 torr.

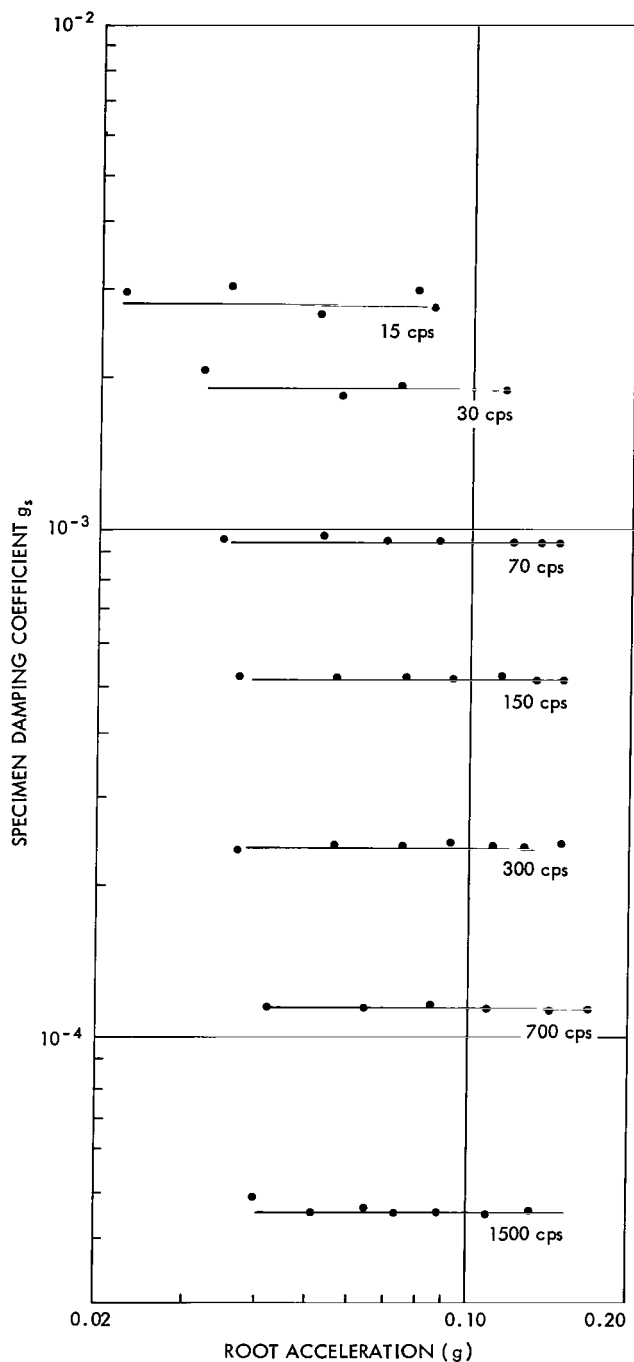


Figure 12—Results for seven resonant beams of 1/10-inch thick aluminum tested in a vacuum of 0.2 torr.

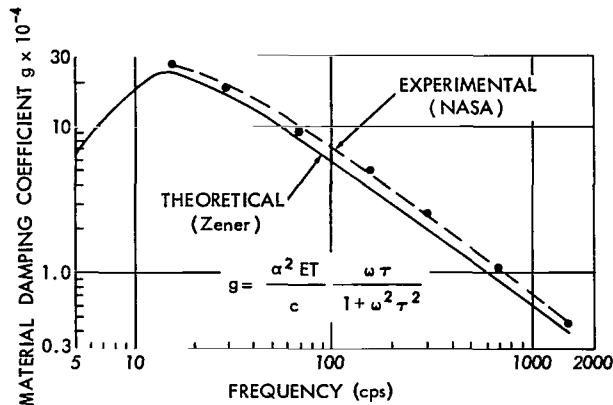


Figure 14—Comparison of damping as calculated by theoretical thermal relaxation equations and as measured experimentally (for 0.10-inch thick aluminum beams).

Figures 14 and 15 show good correlation with Zener's expression; (Equation 3).

The following conclusions may be drawn from the results obtained.

1. A unique, simple and accurate technique has been developed for measuring material damping.
2. Material damping of Aluminum 2024-T4 is (1) independent of stress amplitudes up to 20,000 psi and (2) frequency dependent in the range 15-1500 cps.
3. Material damping of Aluminum 2024-T4 is independent of stress history at stresses below 20,000 psi.
4. Material damping of Aluminum 2024-T4 can be quantitatively evaluated by the Zener relation, $g = (\alpha^2 ET/c) (\omega\tau / (1 + \omega^2\tau^2))$.
5. Air damping as observed during these tests provides a significant contribution to total damping and may be as much as 10 times greater than material damping.

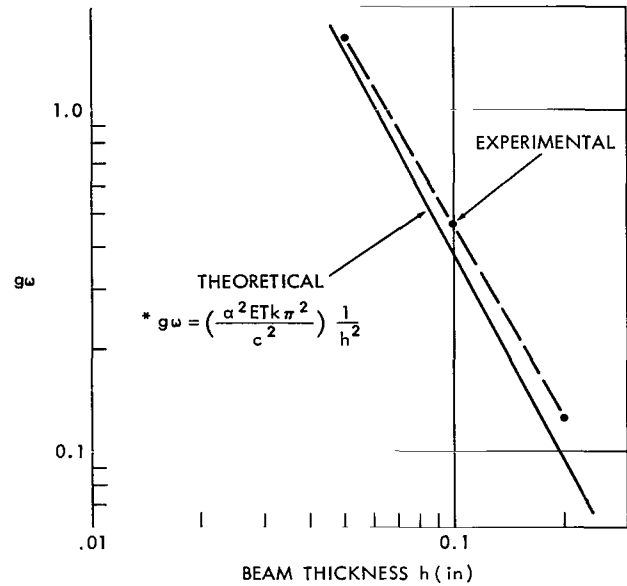


Figure 15—Comparison of $g\omega$ as measured on three thicknesses of beams with theoretical $g\omega$ for beams in the same thickness range ($\omega^2\tau^2 \gg 1$).

$$\begin{aligned}
 *g &= \frac{\alpha^2 ET}{c} \frac{\omega\tau}{1 + \omega^2\tau^2} \\
 &= \frac{\alpha^2 ET}{c} \frac{1}{\omega\tau} \text{ FOR } \omega^2\tau^2 \gg 1 \\
 \tau &= \frac{h^2 c}{\pi^2 k}
 \end{aligned}$$

Table 3
Beam Damping Measurements in Air

Resonant Frequency		Beam Thickness h (in.)	Calc. Root Stress σ_r (psi)	Root Acceleration a (gravity units)	Displacement Double Amplitude		Q	Damping Coefficient $\xi_s \times 10^4$
Nominal (cps)	Actual (cps)				Root $\delta_o \times 10^3$ (in.)	Tip δ_{Res} (in.)		
15	15.16	0.100	4800	.056	4.79	1.02	136	73.4
			7200	.104	8.88	1.54	110	90.6
			9600	.167	14.3	2.05	91.8	109
			12000	.234	20.0	2.56	81.6	123
			14400	.297	25.1	3.07	78.0	128
			16800	.354	30.1	3.58	75.9	132
			19200	.448	38.3	4.09	68.2	147
30	30.18	0.100	4700	.058	1.24	0.505	259	38.6
			7200	.121	2.61	0.768	187	53.6
			9500	.189	4.05	1.01	160	62.6
			12000	.290	6.23	1.28	131	76.1
			14300	.373	8.02	1.53	122	82.1
			16700	.475	10.2	1.79	112	89.3
			19200	.561	12.1	2.05	109	92.1
70	71.50	0.100	4700	.0495	0.189	.215	725	13.8
			7100	.0931	0.356	.323	578	17.3
			9400	.157	0.594	.432	465	21.5
			11900	.255	0.977	.543	355	28.2
			14200	.361	1.38	.652	302	33.2
			16700	.471	1.80	.764	270	37.0
			19000	.592	2.26	.873	246	40.7
150	153.2	0.100	4400	.0472	.0392	.0946	1540	6.50
			6600	.0790	.0656	.142	1378	7.26
			8900	.123	.102	.191	1190	8.40
			11100	.173	.144	.237	1052	9.50
			13300	.237	.197	.284	920	10.9
			15800	.333	.275	.337	785	12.8
			18100	.428	.356	.385	690	14.5
300	306.4	0.100	4700	.0511	.0106	.0505	3030	3.30
			7100	.0890	.0185	.0762	2630	3.80
			9500	.130	.0268	.102	2420	4.13
			11900	.176	.0367	.127	2220	4.51
			14300	.242	.0503	.153	1945	5.14
			16700	.307	.0639	.178	1785	5.60
			19100	.386	.0803	.204	1630	6.13
700	715.8	0.100	4800	.065	.00248	.0221	5680	1.76
			7200	.099	.00380	.0331	5550	1.80
			9600	.145	.00552	.0441	5100	1.96
			12000	.202	.00770	.0552	4590	2.18
			14400	.263	.0101	.0661	4180	2.39
			16900	.341	.0130	.0776	3800	2.63
			19000	.407	.0156	.0869	3560	2.81
1500	1571	0.100	4600	.056	.000446	.0098	14050	.712
			6900	.090	.000710	.0148	13300	.752
			9300	.123	.000975	.0199	13020	.768
			11600	.156	.00123	.0248	12900	.776
			14000	.196	.00153	.0298	12420	.805
			16300	.246	.00195	.0348	11390	.878
			18700	.303	.00240	.0399	10620	.942
70	76.25	0.200	4700	.0168	.0565	.200	2260	4.43
			7000	.0303	.102	.297	1865	5.36
			9300	.0483	.162	.397	1565	6.39
			11600	.0725	.241	.498	1315	7.60
			14000	.100	.337	.599	1135	8.82
			16400	.132	.444	.699	1000	9.99
			18700	.173	.581	.799	880	11.4
300	314.6	0.050	4700	.158	.0312	.0507	1040	9.62
			7100	.264	.0521	.0762	935	10.7
			9500	.375	.0739	.101	878	11.4
			11800	.506	.0999	.126	805	12.4
			14200	.677	.134	.152	725	13.8
			16500	.863	.170	.177	662	15.1
			19000	1.11	.216	.203	602	16.6

Table 4
Beam Damping Measurements in Vacuum

Resonant Frequency		Beam Thickness h (in.)	Calc. Root Stress σ_r (psi)	Root Acceleration a (gravity units)	Displacement Double Amplitude		Q	Damping Coefficient $\xi_s \times 10^4$
Nominal (cps)	Actual (cps)				Root $\delta_o \times 10^3$ (in.)	Tip δ_{Res} (in.)		
15	15.18	0.100	4800	.0223	1.89	1.01	342	29.2
			7200	.0345	2.93	1.53	332	30.1
			9600	.0405	3.43	2.04	379	26.4
			12000	.0510	4.33	2.55	376	26.6
			14400	.0632	5.36	3.06	365	27.4
			16800	.0783	6.65	3.57	342	29.2
			19200	.0833	7.07	4.08	369	27.1
30	30.30	0.100	4800	.0307	.660	.510	493	20.27
			7200	.0433	.924	.774	535	18.71
			9600	.0560	1.18	1.02	551	18.13
			12000	.0729	1.56	1.29	527	18.96
			14400	.0870	1.85	1.54	532	18.80
			16700	.101	2.14	1.79	534	18.73
			19300	.115	2.44	2.06	539	18.55
70	71.60	0.100	4800	.0340	.132	.217	1047	9.55
			7300	.0520	.201	.326	1037	9.64
			9700	.0690	.266	.434	1045	9.57
			12100	.0860	.331	.546	1052	9.50
			14500	.103	.395	.656	1059	9.44
			16900	.120	.461	.766	1060	9.43
			19400	.135	.518	.874	1077	9.28
150	153.2	0.100	4500	.0370	.0308	.096	1990	5.02
			6800	.0570	.0474	.145	1960	5.11
			9000	.0760	.0632	.192	1940	5.15
			11300	.0930	.0774	.240	1980	5.05
			13400	.114	.0948	.287	1935	5.17
			15800	.132	.110	.339	1965	5.09
			18000	.149	.124	.384	1980	5.05
300	306.5	0.100	4700	.0360	.0075	.0497	4240	2.36
			7000	.0554	.0115	.0751	4170	2.40
			9400	.0742	.0154	.0999	4140	2.42
			11700	.0925	.0193	.125	4150	2.41
			14000	.111	.0231	.150	4140	2.42
			16300	.128	.0267	.175	4180	2.39
			18800	.150	.0312	.201	4140	2.42
700	716.2	0.100	4800	.0420	.00159	.0218	8770	1.14
			7100	.0630	.00240	.0326	8720	1.15
			9400	.0850	.00323	.0433	8570	1.17
			11900	.107	.00405	.0545	8640	1.16
			14300	.126	.00476	.0654	8770	1.14
			16700	.147	.00558	.0766	8770	1.14
			19200	.169	.00640	.0880	8770	1.14
1500	1572	0.100	4600	.038	.000303	.0098	20600	.485
			6900	.054	.000428	.0147	21900	.456
			9200	.071	.000565	.0197	22200	.450
			11500	.088	.000700	.0246	22400	.446
			13800	.109	.000839	.0295	22500	.445
70	76.26	0.200	16300	.130	.00103	.0348	21600	.463
			4900	.0095	.0326	.212	4150	2.41
			7200	.0137	.0460	.310	4290	2.33
			9700	.0186	.0625	.413	4250	2.35
			12000	.0255	.0856	.513	3880	2.58
			14400	.0319	.107	.616	3660	2.73
			16500	.0368	.124	.706	3650	2.74
300	314.8	0.050	19200	.0453	.152	.821	3450	2.90
			4500	.126	.0248	.0480	1228	8.15
			6800	.191	.0377	.0733	1238	8.08
			9200	.257	.0506	.0980	1233	8.11
			11300	.324	.0639	.121	1205	8.30
			13800	.387	.0763	.147	1230	8.13
			16000	.448	.0884	.171	1233	8.11
			18400	.514	.101	.197	1240	8.07

REFERENCES

1. Crandall, S. H., "On Scaling Laws for Material Damping," National Aeronautics and Space Administration, Washington, D. C., NASA TN-D-1467, December 1962.
2. Zener, C. M., "Elasticity and Anelasticity of Metals," Chicago: University of Chicago, 1948.
3. Vet, M., "Dwell Sweep Correlation Study," Collins Radio Co., Cedar Rapids, Iowa, CER-1582, 1963.
4. Jacobsen, L. S., and Ayre, R. S., "Engineering Vibrations," New York: McGraw-Hill Book Company, 1958.

Appendix A

List of Symbols

a	= acceleration amplitude of beam root
c	= specific heat per unit volume
E	= modulus of elasticity
F	= beam magnification factor
g	= material damping coefficient
g_s	= specimen damping coefficient
h	= thickness of cantilever beam
I	= moment of inertia
k	= thermal conductivity (see page 2)
k_b	= beam stiffness constant
k_v	= vibrator table stiffness constant
l	= beam length
M_r	= bending moment at root of cantilever
M_b	= beam mass
M_v	= vibrator table mass
n	= material constant
P_0	= vibrator table excitation force
Q	= magnification factor at resonance
R	= function of material and mode shape
S	= stress amplitude
S_0	= material constant
T	= absolute temperature
w	= weight of beam per unit length
x_b	= displacement of beam mass with respect to ground
x_v	= displacement of vibrator table mass with respect to ground
\ddot{x}_b	= acceleration of beam mass with respect to ground
\ddot{x}_v	= acceleration of vibrator table mass with respect to ground
α	= coefficient of linear expansion
δ_0	= input root displacement at resonance
δ_r	= output tip displacement at resonance
δ_x	= displacement of beam at a distance x from the root
ρ	= mass density of beam material
σ_r	= stress at cantilever root
τ	= relaxation time for temperature equalization in a specimen by transverse heat flow
Ω	= natural frequency of vibrator table
ω	= vibration frequency (radians)
ω_1	= first mode resonant frequency
ω_b	= natural resonant frequency of beam